

Vapor Transport of a Volatile Solvent for a Multicomponent Aerosol Droplet

James Q. Feng

November 6, 2021

Optomec, Inc., 2575 University Avenue, Suite #135, St. Paul, Minnesota 55114, USA
email: jfeng@optomec.com

Abstract

This work presents analytical formulas derived for evaluating vapor transport of a volatile solvent for an isolated multicomponent droplet in a quiescent environment, based on quasi-steady-state approximation. Among multiple solvent components, only one component is considered to be much more volatile than the rest such that other components are assumed to be nonvolatile remaining unchanged in the droplet during the process of (single-component) volatile solvent evaporation or condensation. For evaporating droplet, the droplet size often initially decreases following the familiar “ d^2 law” at an accelerated rate. But toward the end, the rate of droplet size change diminishes due to the presence of nonvolatile cosolvent. Such an acceleration-deceleration reversal behavior is unique for evaporating multicomponent droplet, while the droplet of pure solvent has an accelerated rate of size change all the way through the end. This reversal behavior is also reflected in the droplet surface temperature evolution as “S-shaped” curves. However, a closer mathematical examination of conditions for acceleration-deceleration reversal indicates that the acceleration phase may disappear when the amount of nonvolatile cosolvent is relatively small and ambient vapor pressure is relatively high. Because the net effect of adding nonvolatile cosolvent is to reduce the mole fraction of the volatile solvent such that the saturation vapor pressure is lowered, vapor condensation onto the multicomponent droplet is predicted to occur when the ambient vapor pressure is subsaturated with respect to that for the pure volatile solvent. In this case, the droplet will grow asymptotically toward a finite size. But when the ambient vapor pressure becomes supersaturated with respect to that for the pure volatile solvent, the condensation growth of droplet can continue indefinitely without bound.

1 Introduction

In Aerosol Jet[®] additive manufacturing, the ink, consisting of both volatile and nonvolatile solvents besides the solids, is atomized into a dense mist of fine aerosol droplets usually about 50 nL/cc or more. The ink mist, with droplets of typical diameters in the range between 1 to 5 μm , is then carried through conditioning

devices to an aerodynamic focusing nozzle for precision material deposition onto a substrate (cf. Zollmer et al., 2006; Kahn, 2007; Christenson et al., 2011). The primary functionality of the volatile component is to reduce ink viscosity so as to enable effective atomization. Once atomized, the ink droplets are desired to have high solid content especially when they arrive at the substrate. Higher solid content corresponds to higher viscosity as preferred for retaining the printed features at high mass deposition rate, which may not be easily achieved with an ink too “runny” on the substrate. Therefore, removal of the volatile component in ink droplets before deposition plays an important role in high-quality Aerosol Jet[®] printing. In fact, the ink for Aerosol Jet[®] printing is typically formulated to contain solvents with one volatile component and one non-volatile component. The reason for having a non-volatile component is, while the volatile component is mostly removed, to retain cohesivity of the printed features for further solidification processing such as controlled drying, sintering, with appropriate annealing.

Because the ink droplets in the Aerosol Jet[®] printing process travel through a transportation channel from the atomizer to the deposition nozzle before arriving the substrate, opportunities are available for “in-flight” droplet solid content adjustment via the channel shape design, selection of mist flow rate and sheath flow rate, variation of the ratio between volatile and nonvolatile solvent components in the ink formulation, etc. Thus, non-contact deposition of ink droplets with high solid content becomes possible with the Aerosol Jet[®] technology, enabling single-pass high-aspect-ratio feature printing. When designing-optimizing an Aerosol Jet[®] printer, formulating an ink, or developing a process recipe for a particular application, understanding the physical principles behind volatile solvent transport for a multicomponent ink droplet becomes practically important with an analytical theory that can provide reasonable estimate of relevant time scales involved therewith.

The main purpose of the present work is to derive analytical formulas for conveniently evaluating the evaporation as well as condensation characteristics of an isolated ink droplet. It can be easily used to provide theoretical guidance to ink formulation as well as Aerosol Jet[®] printing recipe development. For consistent printing performance, relative motions of ink droplets in the Aerosol Jet[®] mist stream are minimized by design as the mist flowing through the deposition nozzle and exposing to a coflowing sheath gas with controllable solvent vapor contents, where substantial droplet evaporation occurs. Thus, a model based on vapor transport of a volatile solvent for an isolated multicomponent droplet in a quiescent surrounding gas is expected to be quite relevant.

In a bigger picture, the evaporation behavior of aerosol droplets is of interested to a variety of applications such as spray drying (Lin and Gentry, 2003), liquid fuel combustion (Aggarwal, 1998), pharmaceutical aerosol drug delivery to the lungs (Peng et al., 2000), atmospheric science (Pruppacher and Klett, 1978), to name a few. It is a subject studied theoretically by many authors (e.g., Maxwell, 1878; Pruppacher and Klett, 1978; Ravindran and Davis, 1982; Kulmala et al., 1993; Widmann and Davis, 1997). Analytical formulas were presented for evaporation of a single component (unitary) droplet (Maxwell, 1878; Pruppacher and Klett, 1978) or evaporation of a two-component (binary) droplet with constant and uniform composition (Kulmala et al., 1993; Vesala et al., 1997). In mathematical derivations, the assumptions of “quasi-steady-state” and “diffusion-controlled” mass transfer have typically been used. Coupled nonlinear equations for multicomponent evaporation of a multicomponent droplet were derived with solutions computed numerically (Ravindran and Davis, 1982; Widmann and Davis, 1997; Wilms, 2005). Comparison between theory and experiment have been presented by Wilms (2005); Davies et al. (2012), among others.

For Aerosol Jet[®] printing, the in-process evaporation of only a single (volatile) solvent component from a multicomponent droplet is of interest for most of the times. Although the involvement of multiple solvent components in the ink droplets makes mathematical derivations somewhat complicated, an analytical formula can still be obtained and can be conveniently used for effective technology development. In what follows, detailed mathematical derivation steps with simplifying assumptions are presented in section 2, followed by results and discussion in section 3 for both evaporating droplet and growing droplet by condensation. Finally, the key predictions are summarized in section 4.

2 Mathematical Derivation

A spherical multicomponent liquid droplet is considered here in a quiescent surrounding gas, with one of its solvent components (the volatile component) evaporating (or condensing) while the amount of other (nonvolatile) components remaining unchanged during the time scale of interest. The ink droplets suitable for Aerosol Jet[®] printing typically have diameters in the range of 1 to 5 μm , containing about 10% volume of solids (whose only role is considered to passively occupy some of the droplet volume). Thus, the size of an ink droplet after complete removal of the volatile solvent should be about half of its original size, still much larger than the mean free path of the surrounding gas molecules under ambient condition. It is therefore not unreasonable to ignore the Knudsen number effect. Similar to Feng (2013), the spherically symmetric mass transfer of the volatile solvent vapor in an incompressible continuous gas medium with density ρ_g and diffusivity D is governed by (Bird et al., 1960, p. 557)

$$\frac{\partial \rho_v}{\partial \hat{t}} + v \frac{\partial \rho_v}{\partial r} = \frac{1}{r^2} \frac{\partial}{\partial r} \left(D \frac{\partial \rho_v}{\partial r} \right) \quad (\hat{R} \leq r < \infty), \quad (1)$$

where ρ_v denotes the mass concentration of the solvent vapor, \hat{t} the time, and r the radial distance from the center of the droplet of radius $\hat{R}(\hat{t})$. To satisfy the equation of continuity while accounting for the effect of volume change during the solvent phase change, the radial velocity v of spherically symmetric incompressible flow is simply (Scriven, 1959)

$$v = \left(1 - \frac{\rho_l}{\rho_g} \right) \left(\frac{\hat{R}}{r} \right)^2 \frac{d\hat{R}}{d\hat{t}}, \quad (2)$$

where ρ_l denotes the liquid density of the solvent under consideration.

At the droplet surface, the mass balance based on Fick's first law of binary diffusion accounting for the bulk flow effect with the gas medium flux being ignored (Bird et al., 1960, p. 502) leads to

$$\frac{d\hat{R}}{d\hat{t}} = \frac{\rho_g D}{\rho_l (\rho_g - \rho_{v,R})} \left(\frac{\partial \rho_v}{\partial r} \right)_{r=\hat{R}}, \quad (3)$$

where $\rho_{v,R}$ denotes the vapor density at droplet surface ($r = \hat{R}$).

For most volatile solvents used in Aerosol Jet[®] inks, the density of solvent vapor is much less than that of gas medium, i.e., $\rho_{v,R} \ll \rho_g$ and the diffusivity D may be treated as a constant. Thus, in (1) the convection term

$$v \frac{\partial \rho_v}{\partial r} = \left(1 - \frac{\rho_l}{\rho_g} \right) \left(\frac{\hat{R}}{r} \right)^2 \frac{\rho_g D}{\rho_l (\rho_g - \rho_{v,R})} \left(\frac{\partial \rho_v}{\partial r} \right)_{r=\hat{R}} \frac{\partial \rho_v}{\partial r} \sim - \frac{\rho_{v,R}}{\rho_g} D \frac{\hat{R}}{r^2} \frac{\partial \rho_v}{\partial r}$$

may be assumed negligible comparing with other terms. Then, with the terms associated to $\rho_{v,R}/\rho_g$ ignored, the solution to (1) leads to mass balance at the droplet surface

$$\frac{d\hat{R}}{d\hat{t}} = - \frac{D(\rho_{v,R} - \rho_{v,\infty})}{\rho_l} \frac{1}{\hat{R}} \left(1 + \frac{\hat{R}}{\sqrt{\pi D \hat{t}}} \right), \quad (4)$$

where $\rho_{v,\infty}$ denotes the ambient vapor density at $r \rightarrow \infty$. Although exact solution to (4) may be derived (cf., Feng, 2013), retaining the complexity due to the transient diffusion flux term $\hat{R}/\sqrt{\pi D \hat{t}}$ seems to be unnecessary because significant change of \hat{R} occurs on a time scale $\sim \rho_l R_0^2 / (\pi D \rho_{v,R})$ (with R_0 denoting the droplet initial radius used here as the characteristic length) which is much greater than $\hat{R}^2 / (\pi D)$ for

$\rho_l \gg \rho_{v,R}$ (i.e., liquid density is much greater than gas density). Hence, the quasi-stationary mass balance equation (4) may be reasonably approximated by a quasi-steady-state equation

$$\frac{d\hat{R}^2}{d\hat{t}} = -\frac{2D(\rho_{v,R} - \rho_{v,\infty})}{\rho_l}, \quad (5)$$

which has the same form as standard expression based on Maxwell continuum transport approximation (e.g., Pruppacher and Klett, 1978; Widmann and Davis, 1997).

As expected (Pruppacher and Klett, 1978, p. 417), vapor transport to and from a droplet also involves substantial heat transfer owing to the release or absorption of heat of phase change, namely the latent heat. The resulting temperature difference between the droplet and its surrounding gas medium causes a flow of sensible heat by thermal diffusion. With the quasi-steady-state approximation, energy balance at the droplet surface leads to

$$(\rho_{v,R} - \rho_{v,\infty}) = \frac{k}{LD}(T_\infty - T_R), \quad (6)$$

where k is the thermal conductivity of the surrounding gas medium, L the latent heat due to volatile solvent phase change, T_∞ and T_R the temperature values at $r \rightarrow \infty$ and $r = \hat{R}$. Moreover, it is usually reasonable to take $\rho_{v,R}$ as the local saturated vapor density at the droplet surface $\rho_{sv,R}$ (with “sv” in the subscript denoting saturated vapor). Making use of the Clausius-Clapeyron relation, for characterizing a discontinuous phase transition between liquid and gas, yields an approximate equation (as justified in Pruppacher and Klett, 1978, p. 420) relating local saturated vapor density difference between $r = \hat{R}$ and $r \rightarrow \infty$ to $(T_R - T_\infty)$ as

$$(\rho_{sv,R} - \rho_{sv,\infty}) = \frac{\rho_{sv,\infty}}{T_\infty} \left(\frac{L}{\mathcal{R}_v T_\infty} - 1 \right) (T_R - T_\infty), \quad (7)$$

where \mathcal{R}_v denotes the (specific) gas constant for the volatile solvent vapor (which can be calculated as the universal gas constant, $8.3143 \times 10^3 \text{ J deg}^{-1} \text{ kmol}^{-1}$, divided by the solvent molecular weight in kg kmol^{-1} .)

Combination of (6) and (7) leads to

$$(\rho_{sv,R} - \rho_{v,\infty}) = \left(1 - \frac{\rho_{v,\infty}}{\rho_{sv,\infty}} \right) \left[\frac{1}{\rho_{sv,\infty}} + \frac{LD}{kT_\infty} \left(\frac{L}{\mathcal{R}_v T_\infty} - 1 \right) \right]^{-1}. \quad (8)$$

Thus, expressing $(\rho_{v,R} - \rho_{v,\infty})$ in terms of corresponding vapor pressure $p_{v,\infty} = \rho_{v,\infty}/(\mathcal{R}_v T_\infty)$, $p_{sv,\infty} = \rho_{sv,\infty}/(\mathcal{R}_v T_\infty)$, and T_∞ yields a more convenient form of (5) as

$$\frac{dR^2}{dt} = -\frac{2}{\pi} \left(1 - \frac{p_{v,\infty}}{p_{sv,\infty}} \right) \left[\frac{\rho_l \mathcal{R}_v T_\infty}{p_{sv,\infty}} + \frac{\rho_l LD}{kT_\infty} \left(\frac{L}{\mathcal{R}_v T_\infty} - 1 \right) \right]^{-1}, \quad (9)$$

where all the variables become dimensionless with $R(t)$ measured in units of the droplet initial (dimensional) radius R_0 and t in units of $R_0^2/(\pi D)$, i.e., $R \equiv \hat{R}/R_0$ and $t \equiv \hat{t}\pi D/R_0^2$. Clearly, $R(t)$ decreases with t when $p_{v,\infty}/p_{sv,\infty} < 1$ as the solvent is evaporating from the droplet. If the droplet is in a supersaturated environment when $p_{v,\infty}/p_{sv,\infty} > 1$, $R(t)$ would increase with t because in this case the solvent is condensing onto the droplet.

If the droplet of multicomponent solution contains only one volatile component, as Aerosol Jet[®] inks are typically formulated, the saturated vapor pressure $p_{sv,\infty}$ for the volatile solvent becomes a function of its mole fraction x in the solution. Assuming the multicomponent mixture is an ideal solution such that Raoult’s law is applicable, we have

$$p_{sv,\infty} = xp_{sv,\infty}^*, \quad (10)$$

with $p_{sv,\infty}^*$ denoting the saturated vapor pressure of the pure volatile solvent. Substituting (10) to (9) incurs complexity due to the fact that x is a function of $R(t)$. With the (dimensionless) volume of nonvolatile

component of liquid solution in the ink droplet denoted by $4\pi R_n^3/3$ and the total volume remaining in the droplet when the volatile component is completely removed—the remnant volume—by $4\pi R_r^3/3$ (which includes both solids and nonvolatile component of liquid solution), the volume of volatile solvent component should be $4\pi(R^3 - R_r^3)/3$ and

$$\frac{1}{x(t)} = 1 + \frac{\rho_n M_v}{\rho_v M_n} \frac{R_n^3}{R(t)^3 - R_r^3}, \quad (11)$$

where ρ_n and ρ_v , M_n and M_v denote the liquid solvent densities, molecular weights of the nonvolatile and volatile components, respectively. Clearly, the mole fraction x is generally a function of time t during the volatile solvent evaporation, because $R(t)$ changes with time while R_n and R_r remaining as constants.

Incorporating (10) and (11) in (9) yields

$$\frac{dR^2}{dt} = -\frac{2}{\pi} \frac{1 - p_{v,\infty}/p_{*sv,\infty}}{A + B/(R^3 - R_e^3)}, \quad (12)$$

where

$$R_e^3 \equiv R_r^3 + \frac{\rho_n M_v R_n^3 p_{v,\infty}}{\rho_v M_n (p_{*sv,\infty} - p_{v,\infty})}, \quad (13)$$

$$A \equiv \frac{\rho_l L D}{k T_\infty} \left(\frac{L}{\mathcal{R}_v T_\infty} - 1 \right) + \frac{\rho_l \mathcal{R}_v T_\infty}{p_{*sv,\infty}}, \quad (14)$$

and

$$B \equiv \frac{\rho_n M_v R_n^3}{\rho_v M_n} \left(\frac{\rho_l \mathcal{R}_v T_\infty}{p_{*sv,\infty}} + \frac{A p_{v,\infty}}{p_{*sv,\infty} - p_{v,\infty}} \right). \quad (15)$$

An analytical solution to (12), though apparently complicated, can be written as

$$R^2 = 1 - \frac{2t(1 - p_{v,\infty}/p_{*sv,\infty})}{\pi A} + \frac{B}{3AR_e} \left\{ \ln \left[\frac{(1 - R_e)^3 (R^3 - R_e^3)}{(R - R_e)^3 (1 - R_e^3)} \right] - 2\sqrt{3} \left(\tan^{-1} \frac{2R + R_e}{\sqrt{3} R_e} - \tan^{-1} \frac{2 + R_e}{\sqrt{3} R_e} \right) \right\}. \quad (16)$$

Unfortunately, (16) is in an implicit form of R as a function t . However, t can be expressed as an explicit function of R , which make it straightforward to calculate the value of t from a given value of R for generating curves of R versus t .

3 Results and Discussion

Without going to the solution, an examination of (12) suggests the possible situation for $dR^2/dt \rightarrow 0$ as $R \rightarrow R_e$ with R_e denoting the equilibrium droplet radius as defined in (13) for the droplet at thermodynamic equilibrium with ambient vapor pressure $p_{v,\infty}$. Of course, this can only happen in the presence of the nonvolatile component, i.e., when R_n is nonzero such that B is nonzero. In the absence of the nonvolatile cosolvents (i.e., $R_n = 0$) that can influence the equilibrium vapor pressure of the volatile solvent, B disappears and R^2 simply becomes a linear function of t for a droplet containing a single solvent.

While (nondimensional) R_n and R_r are subjected to constraint as $R_n \leq R_r < 1$ (measured in units of droplet initial radius R_0), there is no upper limit to the equilibrium radius R_e . According to (13), however, $R_e > 1$ can only happen when $R_n^3 p_{v,\infty} \neq 0$ in a subsaturated environment, i.e., $p_{v,\infty} \leq p_{*sv,\infty}$, while satisfying the condition $p_{*sv,\infty}/p_{v,\infty} < 1/x(0)$ where

$$\frac{1}{x(0)} = 1 + \frac{\rho_n M_v R_n^3}{\rho_v M_n (1 - R_r^3)}. \quad (17)$$

Table 1: Solvent parameter values under standard ambient condition for density ρ_l (kg m^{-3}), molecular weight M_w (kg kmol^{-1}), saturated vapor pressure $p^*_{sv,\infty}$ (Pa), latent heat of vaporization L (J kg^{-1}), diffusivity in air D ($\text{m}^2 \text{s}^{-1}$), and dimensionless A defined in (14) using the thermal conductivity in air $k = 0.024$ ($\text{J m}^{-1} \text{s}^{-1} \text{K}^{-1}$).

Solvent	ρ_l	M_w	$p^*_{sv,\infty}$	L	D	A
water	1000	18.02	2.99×10^3	2.26×10^6	2.50×10^{-5}	1.67×10^5
butanol	810	74.12	5.53×10^2	7.08×10^5	8.00×10^{-6}	6.21×10^4
EG	1113	62.07	8.00	—	—	—

In the case of $p_{v,\infty} = x(0)p^*_{sv,\infty}$, we have $R_e = 1$ and hence $dR^2/dt = 0$ forever because the ambient vapor pressure equals the saturation value starting from $t = 0$. Volatile solvent evaporation occurs when $R_e < 1$, which makes $R(t)$ ($> R_e$) decreases with time until $R(t) \rightarrow R_e$. Vapor condensation onto the droplet can occur either when $R_e > 1$ such that $R(t)$ ($< R_e$) increases with time until reaching R_e , or when $p_{v,\infty} > p^*_{sv,\infty}$. In a supersaturated environment, namely, $p_{v,\infty} > p^*_{sv,\infty}$, we can have $R_e < 0 \leq R_r < 1$ according to (13), in which case the negative R_e loses its physical meaning, but $dR^2/dt > 0$ as the droplet is growing due to $p_{v,\infty}/p^*_{sv,\infty} > 1$ as indicated by (12). Supersaturated vapor will condense onto any surfaces, such as the channel walls, besides the surface of a multicomponent droplet. Noteworthy here is that (13) also suggests an indefinite growth of droplet (without bound) as $p_{v,\infty} \rightarrow p^*_{sv,\infty}$, because it leads to $R_e \rightarrow \infty$.

For illustrations in this section, water and butanol are used as realistic examples for the volatile solvent, and ethylene glycol (EG) for the nonvolatile solvent. They have actually been used in several Aerosol Jet[®] ink formulations. Table 1 shows the typical parameters for those solvents, where only the liquid solvent density ρ_l and molecular weight M_w are relevant for the nonvolatile ethylene glycol. The ambient temperature T_∞ is assumed to be 300 K and ambient pressure to be 10^5 Pa. Thus, the values of $L/(\mathcal{R}_v T_\infty)$ for water and butanol are 16.3 and 21.0, respectively. As a consequence, the value of $\rho_{sv,R}$ is generally less than $\rho_{sv,\infty}$ according to (8). The values of $\rho_{v,R}/\rho_g$ in (3), which is less than $p_{sv,\infty}/10^5$, are therefore < 0.03 and 0.0055 for water and butanol, as *a posteriori* verification of negligible terms associated with factor $\rho_{v,R}/\rho_g$ in our mathematical derivation.

From (16) it is clear that the effects of nonvolatile cosolvent are proportional to the value of B/A . While the value of A remains constant for a given solvent, the value of B , according to (15), is proportional to the volume fraction of nonvolatile cosolvent R_n^3 (among other factors such as the volatile solvent molecular weight M_v , etc.) Thus, a simple inspection of the physical property values in Table 1 would suggest that a butanol-EG droplet should exhibit much more significant effects of nonvolatile solvents than a water-EG droplet.

3.1 Evaporating Droplet

When the equilibrium radius $R_e < 1$, the volatile solvent will evaporate from the droplet of initial $R = 1$ until $R \rightarrow R_e$. In the absence of the nonvolatile cosolvent, i.e., $R_n = 0$, we have $B = 0$ and (16) recovers the familiar classical “d² law” for evaporation of a single component droplet with a constant dR^2/dt . In this case, the volatile solvent can be completely removed in a finite time

$$t_0 = \frac{\pi A(1 - R_r^2)}{2(1 - p_{v,\infty}/p^*_{sv,\infty})}. \quad (18)$$

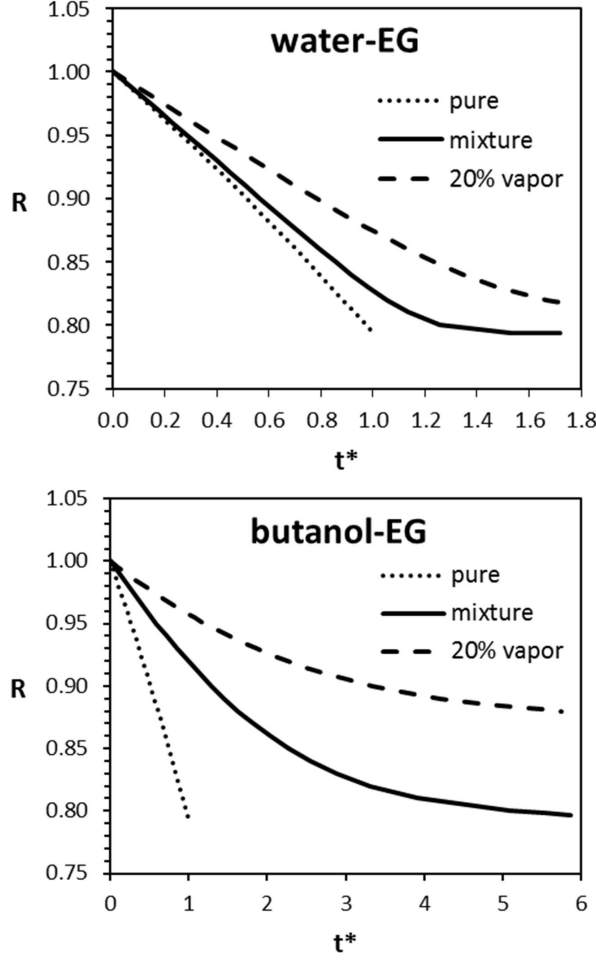


Figure 1: Evaporating droplet radius evolution with time for water-EG and butanol-EG mixtures, with ethylene glycol (EG) serving as the nonvolatile cosolvent with a volume fraction of $R_n^3 = 0.4$. The remnant volume of droplet (excluding that of the volatile solvent) is denoted as $4\pi R_r^3/3$ here in this figure with the remnant volume fraction $R_r^3 = 0.5$. The solid curve and dashed curve correspond to $p_{v,\infty}/p_{sv,\infty}^* = 0$ and 0.2, with $t_{101}^* = 1.23$ and 1.71 for water-EG droplet while $t_{101}^* = 4.81$ and 5.49 for butanol-EG droplet. The dotted curve is for pure volatile solvent with $R_n^3 = 0$ and $R_r^3 = 0.5$ at $p_{v,\infty}/p_{sv,\infty}^* = 0$, as a reference.

A nonzero R_n leads to a nonzero B that causes a fundamental change in the evaporation behavior: the volatile solvent cannot be completely removed in a finite time because now $dR^2/dt \rightarrow 0$ as $R \rightarrow R_e$ due to diminishing mole fraction of the volatile solvent x in the droplet. As a consequence, it is expected to take forever to remove the last bit of the volatile solvent from a droplet in the presence of a nonvolatile cosolvent.

If the droplet has a volume fraction of nonvolatile cosolvent $R_n^3 = 0.4$ and remnant volume fraction $R_r^3 = 0.5$ (namely, $R_r = 0.794$ as the remnant radius), curves of $R(t)$ are shown in Fig. 1 for evaporating droplets of water-EG mixture and butanol-EG mixture with 10% solids and 40% nonvolatile solvents in the initial volume, at $p_{v,\infty}/p_{sv,\infty}^* = 0$ (solid curve) and 0.2 (dashed curve) which is about 25% of $x(0)$ (≈ 0.795) for the water-EG droplet and nearly 50% of $x(0)$ (≈ 0.432) for the butanol-EG droplet. As a reference, also shown in Fig. 1 is the dotted curve representing the case for $R_n = 0$ and $R_r^3 = 0.5$ at $p_{v,\infty}/p_{sv,\infty}^* = 0$ (according to the “d² law”) for a single solvent droplet. For convenience of displaying results, t^* in all figures here is used to denote a normalized time with the value of t_0 in (18) at $p_{v,\infty}/p_{sv,\infty}^* =$

0 such as

$$t^* \equiv \frac{2t}{\pi A(1 - R_r^2)} . \quad (19)$$

Accordingly, the dimensional time corresponding to $t^* = 1$ can be calculated as

$$\frac{A(1 - R_r^2)R_0^2}{2D} , \quad (20)$$

with R_0 and D taking appropriate dimensional values. For example, a water droplet of $R_0 = 10^{-6}$ m (one micron radius, as the typical mean ink droplet radius in the Aerosol Jet[®] mist) containing 50% volume fraction of solids (i.e., a remnant volume fraction of $R_r^3 = 0.5$) will completely evaporate (at $t^* = 1$) in 1.24 milliseconds, according to (20) with parameters in Table 1. But for a butanol droplet of the same size with the same volume fraction of solids, the time for complete evaporation will be 1.43 milliseconds. Increasing the droplet size by a factor of 2 will increase the dimensional time by a factor of 4 for droplets of the same composition, as indicated by (20). If the remnant volume fraction R_r^3 is reduced to 0.2 (or 0.1), the time for complete evaporation of pure solvent-solid droplets would increase by a factor of 1.78 (or 2.12) from that for $R_r^3 = 0.5$.

Strictly speaking, removal of all the volatile solvent from a multicomponent droplet containing non-volatile cosolvent would take forever, i.e., $t^* \rightarrow \infty$. However, it is still of practical interest to evaluate the time for “almost” complete evaporation. Therefore, a time denoted as t_{101}^* for $R(t)$ to reach $1.01 \times R_e$ is used here for evaluating the (finite) time t^* needed for reaching $R \approx R_e$. The value of t_{101}^* can be calculated by substituting $1.01 \times R_e$ for R in (16). For example, the values of t_{101}^* for a water-EG droplet with non-volatile cosolvent volume fraction $R_n^3 = 0.4$ and remnant volume fraction $R_r^3 = 0.5$ at $p_{v,\infty}/p_{sv,\infty}^* = 0$ and 0.2 are 1.23 and 1.71, respectively. But for a butanol-EG droplet with $R_n^3 = 0.4$ and $R_r^3 = 0.5$ at $p_{v,\infty}/p_{sv,\infty}^* = 0$ and 0.2, the values of t_{101}^* become are 4.81 and 5.49, respectively. Thus, it takes a water-EG droplet in Fig. 1 with an initial radius of one micron ($R_0 = 10^{-6}$ m) about ($t_{101}^* \times 1.24$) 1.53 ms and 2.12 ms to “almost” complete the evaporation process at $p_{v,\infty}/p_{sv,\infty}^* = 0$ and 0.2, whereas a butanol-EG droplet (of $R_0 = 10^{-6}$ m) in Fig. 1 needs about ($t_{101}^* \times 1.43$) 6.88 ms and 7.85 ms. Obviously, the presence of the nonvolatile cosolvent (with a volume fraction of $R_n^3 = 0.4$) hinders the volatile solvent evaporation of a butanol-EG droplet much more significantly than that of a water-EG droplet. This is expected from the fact that the value of B/A for the butanol-EG droplet ($= 0.5217$) is much greater than that for the water-EG droplet ($= 0.0358$), at $p_{v,\infty}/p_{sv,\infty}^* = 0$. In the case of $p_{v,\infty}/p_{sv,\infty}^* = 0.2$, the values of the equilibrium radius R_e become 0.810 for the water-EG droplet and 0.872 for the butanol-EG droplet, respectively.

If the volume fraction of nonvolatile solvent is reduced to $R_n^3 = 0.1$ with the remnant volume fraction $R_r^3 = 0.2$, Fig. 2 shows that $R(t)$ for the water-EG droplet almost coincides with that for $R_n = 0$ at $p_{v,\infty}/p_{sv,\infty}^* = 0$ in a grant scale, until $R(t)$ becomes very close to $R_e (= 0.585)$. Although having $p_{v,\infty}/p_{sv,\infty}^* = 0.2$ does not cause much change in the value of R_e (becoming 0.593 with $x(0) = 0.96$), it noticeably reduces the evaporation rate for the water-EG droplet. Despite the substantial reduction of R_n as well as R_r , the butanol-EG droplet still exhibits significant nonvolatile cosolvent effect. Less nonvolatile solvent fraction leads to larger $x(0) (= 0.83)$. Thus, $p_{v,\infty}/p_{sv,\infty}^* = 0.2$ corresponds to $< 25\%$ of vapor equilibrium, which is comparable to the case of water-EG droplet shown in Fig. 1. However, Fig. 2 indicates more significant nonvolatile cosolvent effect than that for the water-EG droplet in Fig. 1, because the value of B/A in this case is 0.130 (still a few times larger than 0.0358 for water-EG in Fig. 1), at $p_{v,\infty}/p_{sv,\infty}^* = 0$. For the case of $p_{v,\infty}/p_{sv,\infty}^* = 0.2$, R_e of the butanol-EG droplet becomes 0.622 as the final equilibrium droplet radius. With $R_n^3 = 0.1$ and $R_r^3 = 0.2$ at $p_{v,\infty}/p_{sv,\infty}^* = 0$ and 0.2, the values of t_{101}^* for a water-EG droplet are 1.06 and 1.37, respectively. But for a butanol-EG droplet they become are 1.94 and 2.57, respectively. Thus, it takes a water-EG droplet in Fig. 2 with an initial radius of one micron ($R_0 = 10^{-6}$ m) about ($t_{101}^* \times 1.24 \times 1.78$) 2.34 ms and 3.02 ms to “almost” complete the evaporation process at $p_{v,\infty}/p_{sv,\infty}^* = 0$ and 0.2, whereas a butanol-EG droplet (of $R_0 = 10^{-6}$ m) in Fig. 2

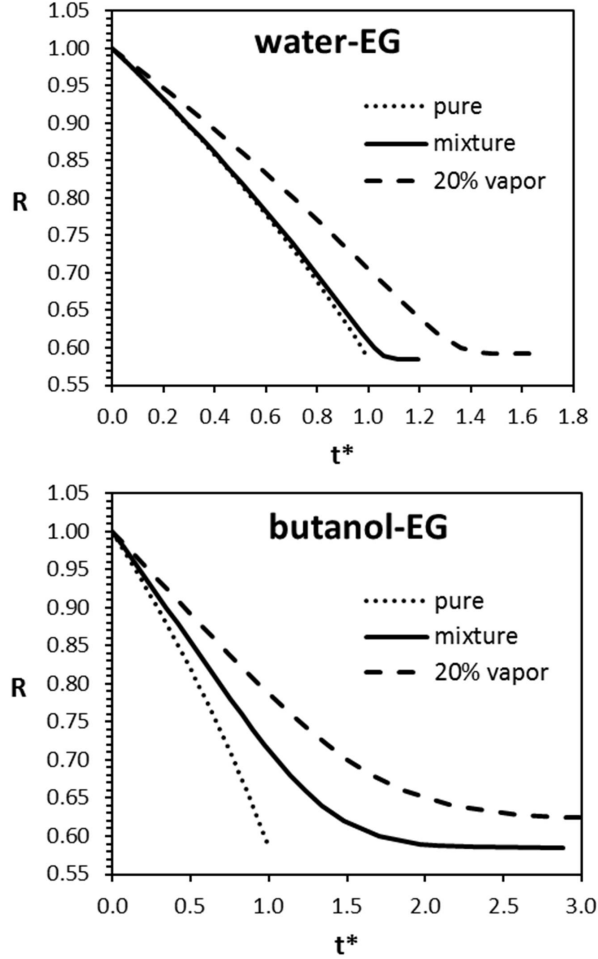


Figure 2: As in Fig. 1 but for $R_n^3 = 0.1$ and $R_r^3 = 0.2$, at $p_{v,\infty}/p_{sv,\infty}^* = 0$ and 0.2 , with $t_{101}^* = 1.06$ and 1.37 for water-EG droplet while $t_{101}^* = 1.94$ and 2.57 for butanol-EG droplet.

needs about $(t_{101}^* \times 1.43 \times 1.78)$ 4.94 ms and 6.54 ms. Interestingly, the reduction of nonvolatile cosolvent volume fraction causes a decrease of time needed for almost complete evaporation of the butanol-EG droplet (comparing that in Fig. 1), while the water-EG droplet needs more time, due to intricate effects of the factor of 1.78 as a consequence of $(1 - R_r^2)$ with a reduction of the value of t_{101}^* for smaller nonvolatile cosolvent volume fraction R_n^3 .

As an apparent general trend shown in Fig.1 and more noticeably so in Fig. 2, the radius of evaporating multicomponent droplet tends to follow the “ d^2 law” with increasing magnitude of slope initially when $R \sim 1$, and then has the magnitude of slope decrease gradually with $dR/dt \rightarrow 0$ as $R \rightarrow R_e$. In other words, evaporating droplet size change is accelerated in the beginning and then decelerated toward the end, if a nonvolatile cosolvent is present. Such an acceleration-deceleration reversal behavior is unique in the presence of nonvolatile cosolvent in the multicomponent droplet, as also noted by previous authors with both experiments and numerical computations (e.g., Widmann and Davis, 1997; Wilms, 2005). In contrast, the d^2 -law behavior of accelerating size reduction all the way to $R = R_e$ is clearly illustrated by the dotted curves for pure solvent cases, which is more obvious in Fig. 2 for the case of $R_n^3 = 0.1$.

To have a closer examination of the conditions for acceleration-deceleration reversal phenomenon, it is

straightforward to derive the formula for d^2R/dt^2 from (12) as

$$\frac{d^2R}{dt^2} = -\frac{(1 - p_{v,\infty}/p^*_{sv,\infty})^2(R^3 - R_e^3)}{\pi^2 R^2 [A(R^3 - R_e^3) + B]^3} \left[A(R^3 - R_e^3)^2 - 2B(R^3 - R_e^3) - 3BR_e^3 \right], \quad (21)$$

which indicates an inflexion point ($d^2R/dt^2 = 0$) for $R^3 > R_e^3$ at $R = R_i$ with

$$R_i^3 = R_e^3 + \frac{B}{A} \left(\sqrt{1 + \frac{3AR_e^3}{B}} - 1 \right). \quad (22)$$

Thus, we have $d^2R/dt^2 < 0$ for $R > R_i$ and $d^2R/dt^2 > 0$ for $R < R_i$ with $d^2R/dt^2 \rightarrow 0$ as $R \rightarrow R_e$. In an explicit form (22) suggests that the value of R_i increases with B which increases with $p_{v,\infty}/p^*_{sv,\infty}$, among others. It is theoretically possible for R_i to become greater than 1. When that happens, the droplet evaporation process would not exhibit the acceleration-deceleration reversal behavior; the droplet radius reduction process should show a decelerating rate all the way to the end. An evaluation of R_i according to (22) shows that $R_i = 0.887$ and 0.929 at $p_{v,\infty}/p^*_{sv,\infty} = 0$ and 0.2 for the water-EG droplet in Fig. 1, which indeed exhibits the acceleration-deceleration reversal behavior (because $R_i < 1$). But for the butanol-EG droplet in Fig. 1, which do not seems to show obvious acceleration-deceleration reversal, the values of R_i are 1.002 and 1.101 (both are greater than 1) at $p_{v,\infty}/p^*_{sv,\infty} = 0$ and 0.2 . With a reduction of B via reduction of the nonvolatile cosolvent volume fraction R_n^3 to 0.1 as in Fig. 2 (for $R_r^3 = 0.2$, where the acceleration-deceleration reversal is observable), the butanol-EG droplet would have $R_i = 0.723$ and 0.773 at $p_{v,\infty}/p^*_{sv,\infty} = 0$ and 0.2 .

3.2 Condensational Growth of Droplet

Droplet can grow by condensation of the volatile solvent vapor when $p_{v,\infty}/p^*_{sv,\infty} > x(0)$, which corresponds to $R_e > 1$ if $p_{v,\infty}/p^*_{sv,\infty} \leq 1$, again until R reaches R_e . According to (13), $R_e \rightarrow \infty$ at the limit of $p_{v,\infty}/p^*_{sv,\infty} = 1$, suggesting that the droplet can grow indefinitely without bound. However, for $p_{v,\infty}/p^*_{sv,\infty} > 1$, the negative value of R_e loses physical meaning, as it monotonically increases from $-\infty$ with $p_{v,\infty}$ increasing from $p^*_{sv,\infty}$. It should be noted that (13) can be rewritten as $p_{v,\infty}/p^*_{sv,\infty} = \{1 + \rho_n M_v R_n^3 / [\rho_v M_n (R_e^3 - R_r^3)]\}^{-1}$, which can only relate to the volatile solvent mole fraction x when $p_{v,\infty}/p^*_{sv,\infty} \leq 1$, corresponding to $R_e \geq R_r$. In that case, the droplet size will change until $R = R_e$ when the volatile solvent mole fraction $x(t)$ in the droplet reaches the thermodynamic equilibrium value of $p_{v,\infty}/p^*_{sv,\infty}$.

The condensation growth behavior of a butanol-EG droplet is illustrated in Fig. 3, with nonvolatile cosolvent volume fraction $R_n^3 = 0.4$ and remnant volume fraction $R_r^3 = 0.5$, at $p_{v,\infty}/p^*_{sv,\infty} = 0.6, 0.9, 0.99, 1.01, \text{ and } 1.10$. Because the value of $x(0)$ is 0.432 for $R_n^3 = 0.4$ and $R_r^3 = 0.5$, condensation growth will occur whenever $p_{v,\infty}/p^*_{sv,\infty} > 0.432$. The values of R_e corresponding to $p_{v,\infty}/p^*_{sv,\infty} = 0.6, 0.9, \text{ and } 0.99$ are $1.14, 1.86, \text{ and } 4.03$, respectively. Thus, when $p_{v,\infty}/p^*_{sv,\infty} < 1$, condensation growth of a multicomponent droplet will practically reach a finite size R_e (as $t^* \rightarrow \infty$). In other words, a multicomponent droplet cannot grow indefinitely without bound in an environment of $p_{v,\infty}/p^*_{sv,\infty} < 1$ by vapor condensation. Useful insights may be gained, however, by examining the normalized time $t_{0.99}^*$ for R to reach $0.99 \times R_r$, similar to $t_{1.01}^*$ for evaporating droplet. For example, with $R_n^3 = 0.4$ and $R_r^3 = 0.5$, the values of $t_{0.99}^*$ are $13, 172, \text{ and } 8131$, for $p_{v,\infty}/p^*_{sv,\infty} = 0.6, 0.9, \text{ and } 0.99$, respectively. Thus, a butanol-EG droplet of $R_0 = 10^{-6}$ m will take $0.029, 0.385, \text{ and } 18.295$ seconds to reach $0.99 \times R_r$ for $p_{v,\infty}/p^*_{sv,\infty} = 0.6, 0.9, \text{ and } 0.99$, given that $t^* = 1$ corresponding to 2.25 milliseconds. When $p_{v,\infty}/p^*_{sv,\infty} \geq 1$, a multicomponent droplet will grow indefinitely with time, as seen in Fig. 3 for $p_{v,\infty}/p^*_{sv,\infty} = 1.01$ and 1.10 . In this case, the normalized time t_5^* for $R = 5$ might be a useful measure as the time needed for a droplet to grow 125 times of its initial volume. For a butanol-EG droplet with $R_n^3 = 0.4$ and $R_r^3 = 0.5$, the

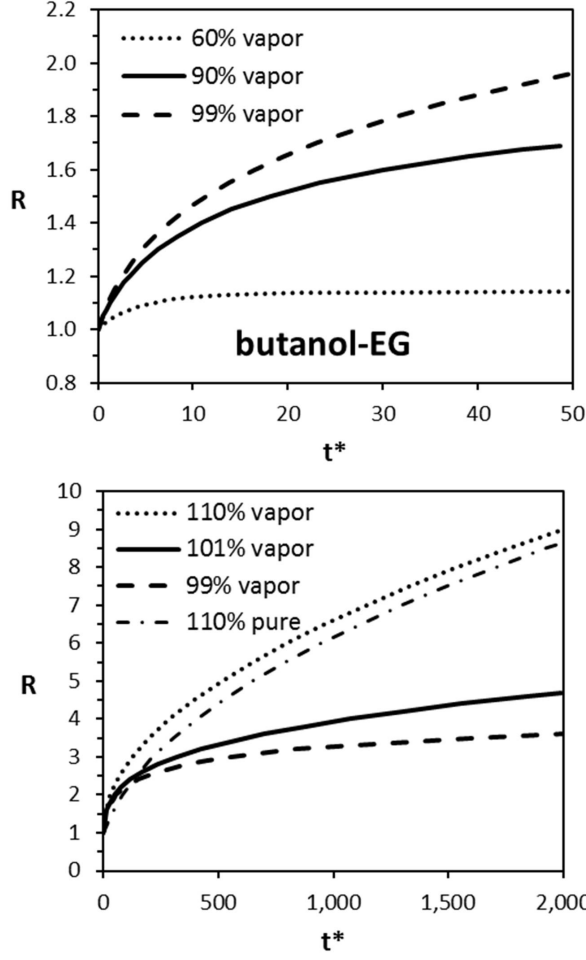


Figure 3: As in Fig. 1 (with nonvolatile cosolvent volume fraction $R_n^3 = 0.4$ and remnant volume fraction $R_r^3 = 0.5$) but only for butanol-EG droplet at $p_{v,\infty}/p_{sv,\infty}^* = 0.6, 0.9, 0.99, 1.01,$ and 1.10 to illustrate characteristics of condensation growth of a multicomponent droplet. The dot-dash curve labeled “110% pure” is for a reference case with $R_n^3 = 0$ and $R_r^3 = 0.5$ for pure butanol droplet at $p_{v,\infty}/p_{sv,\infty}^* = 1.10$. The values of t_{099}^* at $p_{v,\infty}/p_{sv,\infty}^* = 0.6, 0.9,$ and 0.99 are 13, 172, and 8131. The values of t_5^* at $p_{v,\infty}/p_{sv,\infty}^* = 1.01$ and 1.10 are 2488, and 514. For the dot-dash curve with $R_n = 0$, the value of t_5^* is 649.

values of t_5^* are 2488 and 514, for $p_{v,\infty}/p_{sv,\infty}^* = 1.01$ and 1.10 , respectively. As a reference, a dot-dash curve is also shown in Fig. 3 for a pure butanol droplet (with $R_n^3 = 0$ and $R_r^3 = 0.5$) at $p_{v,\infty}/p_{sv,\infty}^* = 1.10$, indicating slower growth of $R(t)$ than a butanol-EG droplet especially near $t^* = 0$. The value of t_5^* for the dot-dash curve with $R_n = 0$ in Fig. 3 is 649. But with time, the dotted curve will converge to the dot-dash curve, because as the droplet grows indefinitely its volatile solvent mole fraction will increase toward unity asymptotically.

Similar to Fig. 3, the condensation growth behavior of water-EG droplet is shown in Fig. 4. Because it is necessary to have $p_{v,\infty}/p_{sv,\infty}^* > 0.795$ ($= x(0)$, which is larger than that for the butanol-EG mixture) for condensation growth to occur, a water-EG droplet is expected to grow at a slower rate than a butanol-EG droplet as reflected in a comparison of Fig.3 and Fig. 4. For the water-EG droplet with $R_n^3 = 0.4$ and $R_r^3 = 0.5$, the value of t_{099}^* is 2660 for $p_{v,\infty}/p_{sv,\infty}^* = 0.99$, and the values of t_5^* are 4471 and 600, for

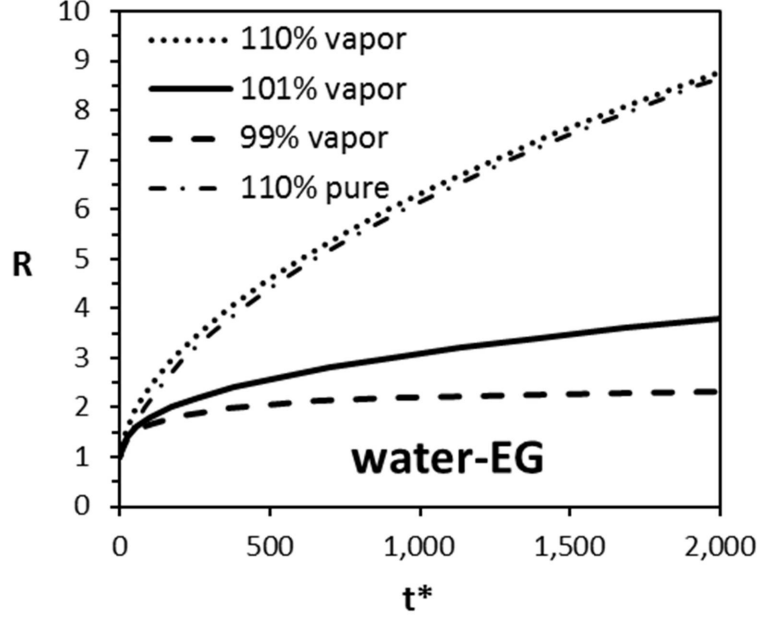


Figure 4: As in Fig. 3 but for water-EG droplet at $p_{v,\infty}/p_{sv,\infty}^* = 0.99, 1.01,$ and 1.10 . The value of $t_{0.99}^*$ at $p_{v,\infty}/p_{sv,\infty}^* = 0.99$ is 2660. The values of t_5^* at $p_{v,\infty}/p_{sv,\infty}^* = 1.01$ and 1.10 are 4471, and 600. For the dot-dash reference curve with $R_n = 0$, the value of t_5^* is 649.

$p_{v,\infty}/p_{sv,\infty}^* = 1.01$ and 1.10 , respectively. The value of t_5^* for the dot-dash curve with $R_n = 0$ in Fig. 4 is 649 again (as independent of solvent type in the absence of nonvolatile cosolvent due to the definition of normalized time). A less significant difference between curves for the water-EG droplet (dotted) and pure water droplet (dot-dash) also suggests a weaker nonvolatile cosolvent effect on vapor transport for the water-EG droplet than for butanol-EG droplet, as noticed in the case of evaporating droplet.

In general, condensation growth of droplet exhibits shallower slope than evaporating droplet, as illustrated by comparing time scales shown in Fig. 1, Fig. 2 with that in Fig. 3, Fig.4. This may be explained by the fact that $dR/dt \sim 1/R$ according to (12), indicating a tendency of accelerating droplet size reduction during evaporation while decelerating droplet size growth during condensation. In the case of condensation growth, the volatile solvent mole fraction increases with time and therefore the nonvolatile cosolvent effect decreases progressively in the process. Thus, no physical mechanism exists for the acceleration-deceleration reversal phenomenon in condensational growth of a multicomponent droplet. While the presence of nonvolatile cosolvents tends to hinder droplet evaporation, it consistently enhances the condensational growth

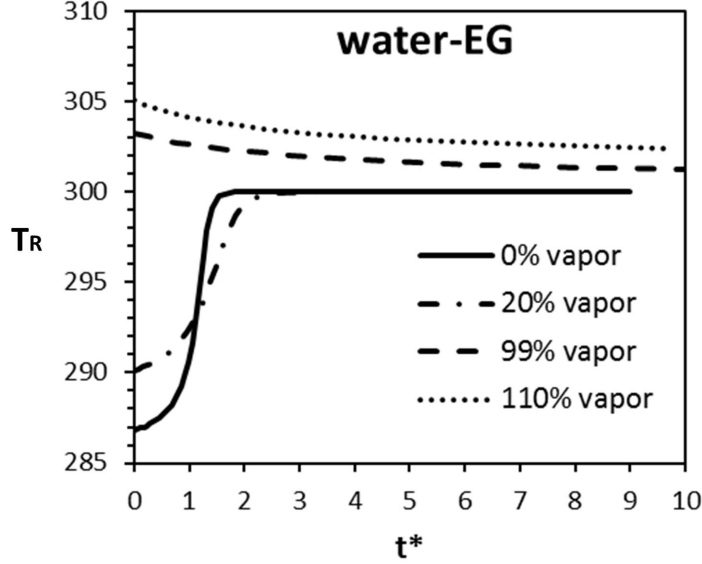


Figure 5: Surface temperature T_R evolution for water-EG droplet with nonvolatile cosolvent volume fraction $R_n^3 = 0.4$ and remnant volume fraction $R_r^3 = 0.5$, at $p_{v,\infty}/p_{sv,\infty}^* = 0$ (solid), 0.2 (dot-dash), 0.99 (dashed), and 1.10 (dotted) according to (23).

rate of a multicomponent droplet due to the effective reduction of saturation vapor pressure of the volatile solvent.

3.3 Droplet Surface Temperature

In theoretical analysis, an explicit expression of the local temperature at droplet surface is sometimes useful (e.g., Kulmala et al., 1993; Vesala et al., 1997). As a by-product of the mathematical derivation, the formula for local temperature at the multicomponent droplet surface T_R , according to (6) and (8), can be obtained as

$$T_R = T_\infty \left(1 + \frac{\pi \rho_l L D}{2kT_\infty} \frac{dR^2}{dt} \right) = T_\infty \left[1 - \frac{\rho_l L D}{kT_\infty} \frac{1 - p_{v,\infty}/p_{sv,\infty}^*}{A + B/(R^3 - R_e^3)} \right], \quad (23)$$

with dR^2/dt , R_e^3 , A , and B given by (12)—(15). Because $B = 0$ when $R_n = 0$, droplet surface temperature T_R remains constant because $dR^2/dt = \text{constant}$ in the absence of the nonvolatile cosolvent.

For a water droplet ($R_n = 0$) at $p_{v,\infty}/p^*_{sv,\infty} = 0, 0.2, 0.99,$ and 1.10 with $T_\infty = 300$ K, its surface temperature $T_R = 285.87, 288.69, 299.86,$ and 301.41 K, respectively. The presence of nonvolatile cosolvent leads to a time-dependent T_R for dR^2/dt is not a constant anymore. Fig. 5 shows the curves of $T_R(t^*)$ for water-EG droplet with $R_n^3 = 0.4$ and $R_r^3 = 0.5$ at $p_{v,\infty}/p^*_{sv,\infty} = 0$ (solid), 0.2 (dot-dash), 0.99 (dashed), and 1.10 (dotted). For $p_{v,\infty}/p^*_{sv,\infty} < 1$, each curve approaches the asymptotic value 300 K as $dR^2/dt \rightarrow 0$ with increasing t^* , because the diminishing rate for vapor transport leads to an isothermal process. For $p_{v,\infty}/p^*_{sv,\infty} = 1.10 (> 1)$ with $R_n^3 = 0.4$ and $R_r^3 = 0.5$ (dotted curve in Fig. 5), the value of T_R asymptotically approaches 301.41 K (> 300 K) due to a non-diminishing dR^2/dt even as $R \rightarrow \infty$ where $dR^2/dt \rightarrow 2(p_{v,\infty}/p^*_{sv,\infty} - 1)/(\pi A)$. This phenomenon is generally true for $p_{v,\infty}/p^*_{sv,\infty} > 1$ according to (12). The variation of surface temperature T_R appears to be much more dramatic for evaporating droplet than growing droplet by condensation. The ‘‘S-shape’’ curves in Fig. 5 for evaporating multicomponent droplet are consistent with the acceleration-deceleration reversal behavior exhibited in $R(t^*)$ curves in Fig. 1 and Fig. 2. Without the acceleration-deceleration reversal, the surface temperature evolution curves $T_R(t^*)$ for a droplet during condensational growth appear less eventful.

4 Summary

Analytical formulas are derived in the present work for evaluating vapor transport of a volatile solvent for an isolated multicomponent droplet in a quiescent environment, based on quasi-steady-state approximation. Among multiple solvent components, only one component is considered to be much more volatile than the rest such that other components are assumed to remain unchanged in the droplet during the process of volatile solvent evaporation or condensation. With direct application to the Aerosol Jet[®] printing in mind, simplifications were made justifiably for ink droplet diameter around a range of 1 to $5 \mu\text{m}$ such as ignoring the Knudsen number effect, negligible vapor mass concentration compared with the ambient gas density, as well as applicability of Raoult’s law for an ideal solution of multicomponent solvent mixture. The form of derived equation for dR^2/dt suggests that in the presence of nonvolatile cosolvent, the rate of droplet size change diminishes as the amount of volatile solvent in the droplet approaches equilibrium value with the ambient vapor pressure ($R \rightarrow R_e$). In the absence of nonvolatile cosolvent, the droplet radius R changes according to the familiar ‘‘ d^2 law’’, which is recovered from the general formula derived herewith when the volume fraction of nonvolatile cosolvent becomes zero ($R_n = 0$).

In the case of evaporating droplet, the radius $R(t^*)$ initially follows the ‘‘ d^2 law’’ near $R(0) = 1$ with an accelerated rate of change. However, the presence of nonvolatile cosolvent is predicted to continuously reduce the rate of evaporation as the mole fraction of the volatile solvent keeps decreasing. According to Raoult’s law, decreasing the mole fraction effectively corresponds to a reduction of saturation vapor pressure for the volatile solvent and thereby weakens the driving force for evaporation. Thus, the magnitude of droplet size change is eventually decelerated toward the end with $dR/dt \rightarrow 0$ as $R \rightarrow R_e$. Such an acceleration-deceleration reversal behavior in the droplet size change is unique in the presence of nonvolatile cosolvent, while the droplet of pure solvent follows the d^2 law of accelerating size reduction all the way through the end. A closer examination of the explicit formula for d^2R/dt^2 , however, indicates that the acceleration phase may disappear when the nonvolatile cosolvent volume fraction R_n^3 is small and the ambient vapor pressure $p_{v,\infty}$ is relatively high.

Because the net effect of adding nonvolatile cosolvent is to reduce the mole fraction of the volatile solvent such that the saturation vapor pressure is lowered, vapor condensation onto the multicomponent droplet is predicted to occur when the ambient vapor pressure is subsaturated with respect to that for the pure volatile solvent. In this case, the droplet will grow asymptotically toward a finite size $R = R_e (> 1)$. Such restricted growth of droplet by condensation is unique only when the nonvolatile cosolvent is present in the multicomponent droplet. But when the ambient vapor pressure becomes supersaturated with respect to that for the pure volatile solvent, the condensation growth of droplet can continue indefinitely without

bound. Condensation growth of droplet generally exhibits shallower slope than evaporating droplet because the droplet size change is continuously decelerated with time as illustrated in figures of $R(t^*)$ and $T_R(t^*)$.

The effects of nonvolatile cosolvent on the volatile solvent evaporation-condensation characteristics predicted here should occur with general multicomponent droplets, in view of the fact that most multicomponent mixtures contain cosolvents with different volatilities. It is expected more often than not to observe a single component of the most volatile solvent evaporating or condensing at a much shorter time scale than the other cosolvents. Thus, the formulas derived here may become applicable to more general situations with multicomponent droplets as long as the evaporation-condensation time scales for different components differ substantially.

Acknowledgments

The author would like to thank John Lees for encouragement and guidance, and Dr. Mike Renn, Dr. Kurt Christenson, Jason Paulsen, as well as many other Optomec colleagues, for helpful technical discussions.

References

- Aggarwal, S. K. (1998). A review of spray ignition phenomena: Present status and future research. *Prog. Energy Combust. Sci.* 24:565–600
- Bird, R. B., Stewart, W. E., and Lightfoot, E. N. (1960). *Transport Phenomena*. John Wiley, New York
- Christenson, K. K., Paulsen, J.A., Renn, M.J., McDonald, K., and Bourassa, J. (2011). Direct printing of circuit boards using Aerosol Jet[®]. *Proc. NIP 27 Digital Fabric.* 433–436
- Davies, J. F., Haddrell, A. E., and Reid, J. P. (2012). Time-resolved measurements of the evaporation of volatile components from single aerosol droplets. *Aerosol Sci. Technol.* 46(6):666–677
- Feng, J. Q. (2013). Diffusion-controlled quasi-stationary mass transfer for an isolated spherical particle in an unbound medium. *Chem. Eng. Comm.* 200:1:65–76
- Kahn, B. E. (2007). The M³D aerosol jet system, an alternative to inkjet printing for printed electronics. *Organic and Printed Electronics.* 1:14–17
- Kulmala, M., Vesala, T., and Wagner, P.E. (1993). An analytical expression for the rate of binary condensational particle growth. *Proc. R. Soc. Lond. A* 441:589–601
- Lin, J.-C. and Gentry, J. W. (2003). Spray drying drop morphology: Experimental study. *Aerosol Sci. Technol.* 37:15–32
- Maxwell, J. C. (1878). Diffusion, in *Encyclopaedia Britannica*, Vol. 7 (9th ed.), London, 214–221
- Peng, C., Chow, A. H. L., and Chan, C. K. (2000). Study of the hygroscopic properties of selected pharmaceutical aerosols using single particle levitation. *Pharm. Res.* 17:1104–1109
- Pruppacher, H. R. and Klett, J. D. (1978). *Microphysics of Clouds and Precipitation*. D. Reidel Publishing, Dordrecht
- Ravindran, P. and Davis, E. J. (1982). Multicomponent evaporation of single aerosol droplets. *J. Colloid Interf. Sci.* 85:278–288
- Scriven, L. E. (1959). On the dynamics of phase growth. *Chem. Eng. Sci.* 10:1–13

Vesala, T., Kulmala, M., Rudolf, R., Vrtala, A., and Wagner, P. E. (1997). Models for condensational growth and evaporation of binary aerosol particles.. J. Aerosol Sci. 28(4):565–598

Widmann, J. F. and Davis, E. J. (1997). Evaporation of multicomponent droplets. Aerosol Sci. Technol. 27:243–254

Wilms, J. (2005). Evaporation of multicomponent droplets. PhD thesis, University of Stuttgart

Zollmer, V., Muller, M., Renn, M., Busse, M., Wirth, I., Codlinski, D., Kardos, M. (2006). Printing with aerosols: A maskless deposition technique allows high definition printing of a variety of functional materials. Euro. Coating J. 07-08:46–55

Figure Captions

Figure 1: Evaporating droplet radius evolution with time for water-EG and butanol-EG mixtures, with ethylene glycol (EG) serving as the nonvolatile cosolvent with a volume fraction of $R_n^3 = 0.4$. The remnant volume of droplet (excluding that of the volatile solvent) is denoted as $4\pi R_r^3/3$ here in this figure with the remnant volume fraction $R_r^3 = 0.5$. The solid curve and dashed curve correspond to $p_{v,\infty}/p^*_{sv,\infty} = 0$ and 0.2, with $t^*_{101} = 1.23$ and 1.71 for water-EG droplet while $t^*_{101} = 4.81$ and 5.49 for butanol-EG droplet. The dotted curve is for pure volatile solvent with $R_n^3 = 0$ and $R_r^3 = 0.5$ at $p_{v,\infty}/p^*_{sv,\infty} = 0$, as a reference.

Figure 2: As in Fig. 1 but for $R_n^3 = 0.1$ and $R_r^3 = 0.2$, at $p_{v,\infty}/p^*_{sv,\infty} = 0$ and 0.2, with $t^*_{101} = 1.06$ and 1.37 for water-EG droplet while $t^*_{101} = 1.94$ and 2.57 for butanol-EG droplet.

Figure 3: As in Fig. 1 (with nonvolatile cosolvent volume fraction $R_n^3 = 0.4$ and remnant volume fraction $R_r^3 = 0.5$) but only for butanol-EG droplet at $p_{v,\infty}/p^*_{sv,\infty} = 0.6, 0.9, 0.99, 1.01,$ and 1.10 to illustrate characteristics of condensation growth of a multicomponent droplet. The dot-dash curve labeled “110% pure” is for a reference case with $R_n^3 = 0$ and $R_r^3 = 0.5$ for pure butanol droplet at $p_{v,\infty}/p^*_{sv,\infty} = 1.10$. The values of t^*_{099} at $p_{v,\infty}/p^*_{sv,\infty} = 0.6, 0.9,$ and 0.99 are 13, 172, and 8131. The values of t^*_5 at $p_{v,\infty}/p^*_{sv,\infty} = 1.01$ and 1.10 are 2488, and 514. For the dot-dash curve with $R_n = 0$, the value of t^*_5 is 649.

Figure 4: As in Fig. 3 but for water-EG droplet at $p_{v,\infty}/p^*_{sv,\infty} = 0.99, 1.01,$ and 1.10. The value of t^*_{099} at $p_{v,\infty}/p^*_{sv,\infty} = 0.99$ is 2660. The values of t^*_5 at $p_{v,\infty}/p^*_{sv,\infty} = 1.01$ and 1.10 are 4471, and 600. For the dot-dash reference curve with $R_n = 0$, the value of t^*_5 is 649.

Figure 5: Surface temperature T_R evolution for water-EG droplet with nonvolatile cosolvent volume fraction $R_n^3 = 0.4$ and remnant volume fraction $R_r^3 = 0.5$, at $p_{v,\infty}/p^*_{sv,\infty} = 0$ (solid), 0.2 (dot-dash), 0.99 (dashed), and 1.10 (dotted) according to (23).